IEEE Access
Multidisciplinary | Rapid Review | Open Access Journal

Received November 5, 2020, accepted December 6, 2020, date of publication December 9, 2020,
date of current version December 18, 2020.

Digital Object Identifier 10.1109/ACCESS.2020.3043657

Development of Smart Battery Cell Monitoring System and Characterization on a Small-Module Through In-Vehicle Power Line Communication

TIMOTHY A. VINCENT AND JAMES MARCO
Cell Instrumentation Team, WMG, University of Warwick, Coventry CV4 7AL, U.K.
Corresponding author: Timothy A. Vincent (t.a.vincent@warwick.ac.uk)

This work was supported in part by the U.K. Engineering and Physical Sciences Research Council (EPSRC) through the Prosperity Partnership Award under Grant EP/R004927/1.

ABSTRACT Current generation battery electric vehicles lack sufficient systems to monitor battery degradation and aging; consumers demand longer range, faster charging and longer vehicle lifetime. Smart cells, incorporating sensors (e.g. temperature, voltage, and current) offer manufacturers a means to develop longer lasting packs, enabling faster charging and extending range. In this work, instrumented cells (cylindrical, 21700) have been developed. Our novel data logging solution (using power line communication, PLC) permits a comprehensive range of sensors to be installed on each cell. Utilizing the cell bus bars, this reduces the necessary wiring harness size and complexity to instrument packs, which can enable higher density energy storage per volume and weight within the vehicle. In this initial feasibility study, a module (4S2P cells) was tested using two diverse cycles (stepped current, 200 mins × 10 cycles, and transient drive, 50 min) in a laboratory climate chamber. The interface system enables research-prototype or traditional sensors to be connected via the PLC network. Miniature sensors (6 temperature, 1 current, 1 voltage) were installed externally on each cell. Excellent performance was observed from the communication system; maximum 0.003% bit error rate, 50ms message receive time (compared to dedicated wired link). Variation in the measured parameters (originally identical cells, temperature 1.0 °C, voltage 5% state-of-charge, current ∼10%) support the need for improved cell instrumentation to understand cell manufacturing tolerances and aging. This work shows a proof-of-concept study using PLC with instrumented cells, and leads to future work to further reduce the cost and physical size of smart cells.

INDEX TERMS Power line communication PLC, cell sensing, temperature monitoring, module cycling.

I. INTRODUCTION

To reduce pollution from the transport sector, the UK government targets an 80% reduction in CO_2 emissions in the sector by 2050 (relative to 1990, up to 2018 only 3.2% achieved) [1], including banning the sales of internal combustion engine (ICE) cars by at the latest 2040 [2], [3]. To continue the adoption of electric vehicles (EVs), the next generation models must alleviate motorists concerns, where traditionally various negative perceptions are associated with EVs: economic (low residual value), technological (battery degradation), safety (battery fires) and charging (long charging times or access to charging points) [4]. Furthermore, low driving range, termed range anxiety, (Volkswagen EGolf achieves 300km range compared to 600km for ∼50% cheaper ICE counterpart) limits the up-take of current generation EVs. Currently, consumers tend to over-estimate initial purchase cost and running costs, while under-estimating driving range [4].

There are now over 5 million EVs worldwide, a figure that is rapidly increasing in recent years (of which it is estimated 2 million were sold in 2018 alone) [5]. Compared to ICE vehicles however, EVs contribute only a low percent to total vehicle ownership. Data from the UK Government for licensed vehicles from year end 2019 showed petrol and diesel cars still comprise 97.6% of cars licensed for driving on UK roads (EVs contributing a further 2.3%) [6]. Diesel cars, despite growing reports of high emissions [7], still number

The associate editor coordinating the review of this manuscript and approving it for publication was Aijun Yang.

over 39% of the cars on UK roads, perhaps due to longer range and lower litres per 100 km (∼5 l [8], [9]).

A growth in the number of charging stations and their efficiency is helping build the infrastructure necessary to support mass-EV adoption [10], although the battery pack still forms the basis for the majority of negative EV perception. In this work we propose a smart cell monitoring system, demonstrated with proof-of-concept experiments with a small module. Lack of data regarding cell aging and performance while a pack is deployed substantiates consumer concerns, where the longevity of the pack cannot be guaranteed with the current limited monitoring. We view PLC as an underpinning technology to enable future smart instrumented cells. In the short term, these results lead to improved pack development and laboratory studies through improved cell instrumentation, while in longer term, offer a cost effective solution (light-weight, miniature, minimal wiring) to permit the deployment of smart cells in an EV. We show the initial stage, externally instrumenting cells using a PLC network. With the viability of a vehicular PLC system proven, this allows further work including embedding sensors within cells (to demonstrate a deployable smart cell) or expanding the range of sensors tested (to facilitate laboratory studies of module performance).

In this work, our experiments aim to verify the following five hypotheses, to meet our aims to confirm the need and suitability of PLC cell sensor monitoring: (i) Data from the sensors is not corrupted from the PLC transmission process (compared to dedicated wired connection); (ii) The type of miniature sensors used in this work are sufficiently accurate to measure typical cell parameters (i.e. compared to a reference source); (iii) There is sufficient bandwidth to transmit data for eight cells along a single frequency division of the powerline when subjected to transient cycling profiles (iv) Instrumenting a module with one temperature sensor is not suitable to ensure the correct sustainable operation of the module (increases in temperature only detected using array of sensors) and (v) the PLC low bandwidth configuration minimises transmission lag to enable sensor data to be received in a reasonable timeframe.

A. EV INSTRUMENTATION BACKGROUND

It is rare for packs inside current generation EVs to contain more than 20 temperature sensors (usually thermocouples), often containing far fewer [11]. Without monitoring temperature at an individual cell level, any hot-spots which form inside cells cannot be identified. Differential heat generation leads to uneven current distributions (within parallel connections), causing accelerated aging. This effect is compounded if a cell is of lower capacity than its neighbours in a pack, which in the worst case can lead to thermal runaway (combustion). We propose an individual smart cell should contain in-situ sensors for temperature, voltage (reference electrode) and current. With these parameters, a cell's aging can be better understood. This data is immediately useful for design and development of future battery packs. Monitoring these values can improve safety (cells which fall outside a defined operating window can be disconnected) and also EV performance (maximum current flow can be safely enabled and maintained when branch currents are measurement between parallel cells, permitting faster charging and discharging, i.e. acceleration).

In terms of EVs, cost, weight and physical size of components are vital specifications. Lithium-ion (Li-ion) chemistry is preferred for EV packs, due to its favourable energy density (>500 Wh/l [12]). It is estimated the specific energy for a Li-ion cell is ∼250 Wh/kg [13]. This is reduced to approximately 150 to 170 Wh/kg when installed in an EV (with cooling and instrumentation hardware), i.e. a typical reduction in 30 to 40% compared to a compact cell alone. It is this reduction in efficiency that could be improved for future electrification of transport (necessity for battery powered aerospace travel). In a typical EV, it is suggested an additional 100 kg mass in the vehicle increases energy consumption by 0.6 kWh/100 km [14].

Power line communication was selected as a solution to installing multiple sensors per cell, without requiring additional cabling outside the module to connect to a management/data logging system. PLC systems are available for domestic networking, operating at the mains voltage (i.e. 230 V in the UK). Utilising PLC in a single battery cell, the varying DC voltage poses one challenge (depending on the cell's state of charge, SoC), where communication must be possible across a voltage range of ∼2.5 to 4.2 V DC. In this manner, it is proposed a single cell could be connected to a test bench for a rapid grading process.

B. PROPOSED SMART CELL MONITORING SYSTEM

In this work, a 4-series 2-parallel (4S2P) configuration of cells (Figure 1), forming a small module is tested with the PLC network. Thereby the pack voltage can potentially vary from 10 to 16.8 V. Commercially available li-ion cells of format 21700 were selected, offering a desired format used by many original equipment manufacturers for future EVs, and reasonable capacity (4 Ah).

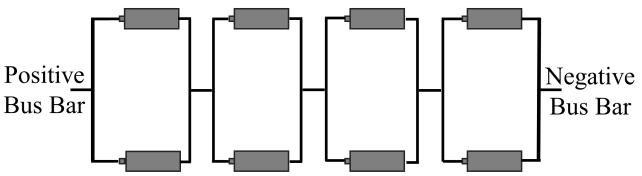

FIGURE 1. Schematic layout of cells connected in 4S2P arrangement.

To enable functionality while the vehicle is running, the PLC system must be robust to noise frequencies (i.e. few hundred kHz to 3 MHz range of transistor switching [15]) while not being detrimental to cell operation in terms of lifetime and performance (diagnostic frequencies 0.01 Hz to 10 kHz are used for electrochemical impedance spectroscopy EIS [16].

EIS could, in future research, be performed in real-time or on-board.

Additionally, the capacitance and impedance of a cell can vary from not only manufacturing tolerances, but they are also related to SoC and age [17], thus vary as the cell charges and discharges. This variation entails phase shift PLC is less suitable for this application, and this work will focus on frequency shift PLC, which will not be significantly influenced.

This work focuses on developing a communication system for sensors installed either on or inside battery cells. We report on the success of the network (considering time taken to receive messages, bit error rate (BER), maximum possible sampling rate/data capacity) and the future steps needed to integrate smart cells into packs, suitable for developing and improving battery pack designs.

Instrumented cells, fitted with various sensors such as thermistors [18], thermocouples [19], optic fibres [20] etc., have been reported. These sensors all rely on dedicated wired connections to interface the sensors to data loggers, requiring complex, bulky and expensive cabling. This limits their use only to battery research laboratories, and prevents their use in various testing scenarios and within real-world EVs.

PLC offers a solution to reduce the wiring required to instrument cells, while offering a flexible platform to install additional sensors (expandable using inputs on a microcontroller). Results from this novel work demonstrate externally instrumented cells, each fitted with 6 temperature sensors (thermistors), a current sensor and a voltage monitor. This article is divided into the following sections: motivation and the need for improved EV battery packs, methodology and experimental setup, results and discussion, and conclusions including our future work.

II. MOTIVATION

A. INSTRUMENTED CELLS

Battery management systems (BMS) monitor and control a pack, for example an EV. Due to current generation EV packs having a limited number of sensors installed, the BMS has restricted data in which to apply algorithms and calculate vital parameters. Without access to cell level sensors, the BMS has to estimate parameters, which contribute to safety critical information, such as temperature calculation [21]. This is particularly difficult, considering the finite processing resources and algorithm complexity (approximations like capacity fade and resistance rise could be neglected).

As regulations regarding EV safety improve, (such as requiring occupants to have a 5 minute warning prior to egress of smoke or heat into the cabin [22]) and the need for longer lifetime battery packs and lower degradation, manufacturers are becoming aware of the need to better instrument battery packs.

Simply installing additional thermocouples into modules is unlikely to alleviate all safety concerns, when it is probable manufacturers must currently over engineer of battery pack designs. The lack of knowledge regarding cell state of health (SoH) prevents faster charging (which can introduce cooling concerns), limiting the appeal of EVs.

As hotspots that can form within cells (small size [23], [24], unlikely to be detected with shared multi-cell sensor), are an indicator of the cell reaching end of life. Excessive hotspots can lead to thermal runaway. Therefore, it is proposed sufficient sensor resolution must be available for each cell, in order for the sensing to be able to provide useful information regarding cell failure prediction. Internal sensing is preferred, where external surface temperature lags core (perhaps up to 10 °C [25]). Protecting the sensors against the harsh chemical environment in a cell provides further challenges.

In this work, a comprehensively instrumented module is tested using research sensors. The microcontroller acquisition channels were not restricted, and traditional sensors can be integrated alongside the miniature devices. In the 4S2P configuration, current is sensed along each branch (via measurements at an individual cell level), enabling a unique understanding of the SoH of the cells and their aging condition.

This work expands upon the single point temperature measurement of a cell, with a string of thermistors distributed along the long axis of the cell surface.

B. PLC

The current solution of dedicated wire per sensor entails configurations cannot simply be scaled up to facilitate reasonable sensor coverage regardless of pack size. PLC offers a scalable solution, where a single modem and microcontroller configuration can interface many sensors. The limitations for PLC are the bandwidth available, considering time and frequency multiplexing are available. Including a microcontroller at the point of sensor interface reduces the load on the data acquisition unit, where basic pre-processing stages (e.g. averaging, peak level identification) can be performed locally. PLC is not restricted to using research sensors, where traditional sensors (e.g. current probes or thermocouples) could be connected to the network in the same manner.

A bi-directional PLC system was selected, without sacrificing physical size, advantageous to enable control of a cell (e.g. to adapt data sampling rates), and potentially control circuitry within the cell.

PLC as a networking tool for battery management has previously been explored [26]–[29], but without the focus on an automotive application, considering experimental data collected with simulated real-world cycling and drive cycle programs.

This work expands previous studies, including work on cell instrumentation and also helps validate the need to monitor voltage and current at an individual cell level. Additionally, results from temperature sensing can help identify the key locations to place temperature sensors within cells to optimise sensor cost vs detection resolution.

Wireless networking for cell monitoring has also previously been studied [30]–[32]. Again, the focus is usually on

either simulation or development of miniature boards for contactless data transmission in a laboratory bench-top environment without testing cell cycling. Wireless transmissions are fundamentally less-secure than wired alternatives, a concern to the automotive industry [33]. Battery packs consist of large quantities of aluminium or composite structures to house the cells. These materials, of course, could attenuate wireless signals; robust testing inside a pack must be performed before wireless technologies could be validated for this application. The physical size of the interface system is challenging to scale to fit a cylindrical smart cell, considering the cumbersome antennas required.

This work demonstrates PLC is capable of instrumented cells at a small module level. Time division multiplexing is sufficient to instrument 8 cells with temperature, voltage and current probes. The system is thoroughly reviewed, as cells are cycled and drive cycles tested.

III. METHODOLOGY

A. EXPERIMENTAL SETUP

A test rig was developed to enable the 8 cells (4S2P layout, capacity 8 Ah) to be securely housed and tested using a battery cycler (FTV 200-60, Bitrode, USA). The instrumentation system comprised a sensor interface board (1 per cell), multiplexer board with PLC modem (1 per 4 cells) and a PLC modem with a data logging computer. A block diagram of the operation of the system is shown in Figure 2. In the current system, one PLC modem was used per 4 cells. This configuration was selected due to the majority of the estimated expensive (∼$8) for an instrumented cell populated PCB currently attributed to the $5 modem, based on manufacturing pricing at time of purchase.

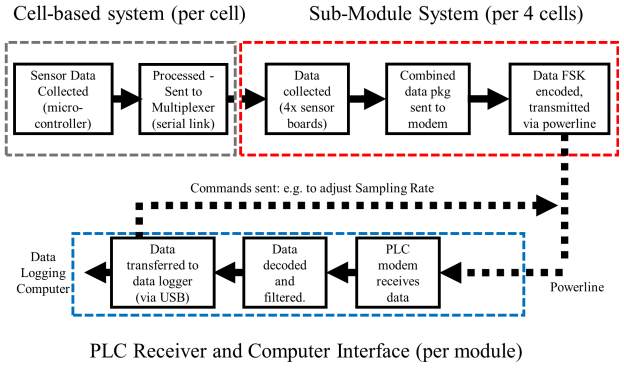

FIGURE 2. Block diagram of PLC system with interface circuitry.

Due to the nature of this research the cell model information and experimental data sets are not available.

In total the system comprises: 8 × 21700 cells, each with 1 current sensor, 1 voltage sensor and 6 thermistor sensors (1 interface board per cell); 2 multiplexer boards, each taking data from 4 sensor boards and connected to a PLC modem; 3 PLC transceiver modems, 2 transmitting data from sensors, and 1 receiving data (at the BMS/data logging computer).

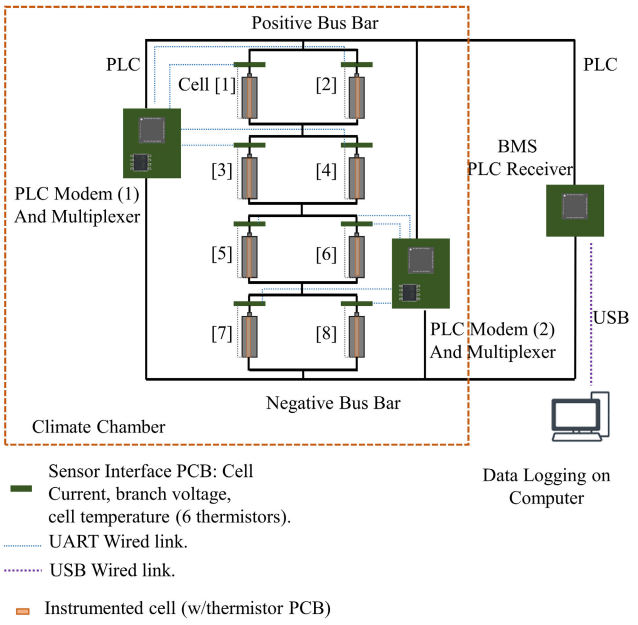

FIGURE 3. Layout of system comprising 8 instrumented cylindrical cells and PLC modem components.

The layout of the system is shown in Figure 3. The module and sensor interface circuitry was placed in a climatic chamber (environmental temperature constant 25 °C), connected to the cycler.

The sensor interface system was designed to enable a PLC modem to be attached per cell, enabling a future wire-free monitoring solution (further work involves developing a cost effective powerline interface). The system is configured to enable each sensor interface board to operate independently, with only data transmitted to a PLC modem. This enables the configuration to be adapted and additional sensors to be tested or trialled on individual cells. Furthermore, it enables only desired cells to be instrumented; i.e. to reduce cost a select arrangement of designated smart cells could be installed in a module.

B. PLC AND SENSOR INTERFACE

A SIG60 PLC modem (Yamar Electronics Ltd, Israel) was selected, as described in our previous work [34]. The relatively low cost modem, is designed for operation inside a vehicle, operating at low DC voltage (10V to 30 V) available in a small package (5 × 5mm 28 pin QFN) [35]. The modem operates at variable bit-rates (9.6 to 115 kbps, 56 kbps selected for reliability), and various channel frequency pairs (5.5 and 6.0 MHz selected, avoiding lower frequency switching noise). The modem offers advantages of a contained line-drive circuitry and PLC modem, although requires relatively bulky external filters.

A low-bandwidth solution was demonstrated, due to the favourable lower power consumption (<150 mW per modem, connected to four cells). Smart real-time adaptable sampling rate is proposed for future work, enabling moderate data

sampling rates, adjustable to faster sampling rates if a feature of interest is detected (e.g. abnormal temperature reading). This reduces the load on the PLC system, and provides the BMS with only the required crucial data values. Initial laboratory tests demonstrated a high bandwidth system required approximately 10× increase in power consumption.

The sensor interface board for each cell comprised the following components: custom PCB, developed with SAMD21G18A microcontroller (Atmel/Microchip Technology Inc., USA), a voltage monitor (microcontroller ADC, 12 bit resolution), a hall-effect current sensor (ACS722LLCTR, Allegro Microsystems, USA) and a voltage regulator (TPS73133DBVR, Texas Instruments, USA). Off-board, an array of 6 thermistors (NCP03WF104F05RL, 0201 imperial size, Murata Manufacturing, Japan) was attached to each interface board. A custom multiplexer board was developed using the same microcontroller with digital isolation circuitry (to account for the different potentials of each cell).

Data were logged at 20 Hz on the sensor interface board and pre-processed (moving average), prior to transmission over the powerline. Adaptable sampling rate was tested, where 4 Hz selected for general measurements (to ensure reliable data transmission within the available bandwidth), 6 Hz available for transient measurements. To check the delay time to receive a message via PLC, and to monitor bit-error rates, a dedicated wired USB connection was logged on cells 7 and 8.

A reference thermocouple was fitted to each cell (Type K, Pico Tech, UK), and logged at 10 Hz. Each sensor was calibrated against reference equipment. The temperature of a climate chamber was varied from 20 to 50 °C in 5 °C steps for the thermistors during calibration. The voltage and current sensors were calibrated against a laboratory power supply. Figure 4 demonstrates the calibration output; (a) shows the calibrated current sensor output (against reference supply readings).

The power supply voltage was varied (3.5, 3.85, 4.2 V) across the range of values expected during the cycling experiments. Charging direction of current flow is indicated by positive values and vice versa for discharging. Error bars indicate standard deviation in current sensor reading at each current step. (b) shows the temperature sensor calibration inside a chamber; the error bars indicate standard deviation at each temperature. The reference sensor for each board is shown by a cross (centre of each measurements set).

The calibrated thermistors were installed on semi-flexible PCBs, onto the cylindrical cells. Figure 5 (a) shows a photograph of the instrumented cell (thermistors out of view on reverse of PCB) and (b) shows the positioning of the devices on the surface of the cell.

C. ASSEMBLED FIXTURE

The assembled unit was installed on an acrylic sheet for safe fitment in the cycling chamber. Figure 6 shows a photograph of the completed module with instrumented cells.

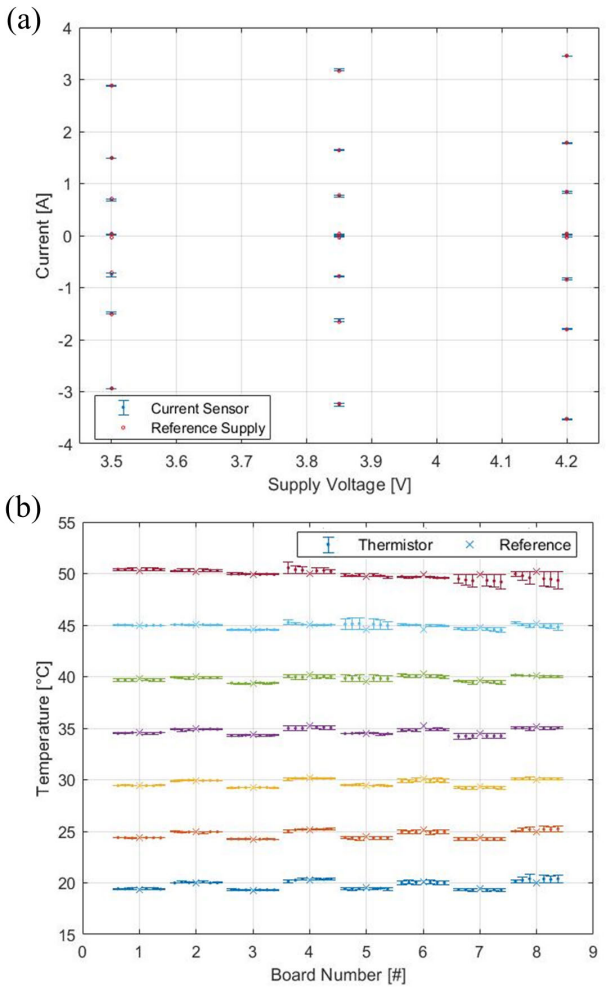

FIGURE 4. Sensors calibrated against reference temperature and current devices, (a) sensor data compared to current measured across resistive load, (b) temperature sensor measurements in climate chamber from 25 to 50 °C.

Interconnecting wires are required for the temperature sensors. A single pair of connections (indicated on the right and left of the photograph) are required for remote communication with the sensors (and for charging and discharging the cells), reducing the wiring needed out of the climate chamber to the data logger.

The multiplexer boards aggregate the data from four interface boards and transmit all the information over the power line. The total data length is 216 bytes per four boards. A total of 9 (resolution 12-bit) sensor records are available per cell (currently allocated as 6 temperature, 1 spare, 1 voltage and 1 current).

If desired, the number of temperature sensors per cell could be reduced, providing capacity for other sensors or cells to be instrumented, without increasing load on the communication network. I.e. each multiplexer board currently collects 36 sensor records, which could alternatively be split 3 records per cell, enabling 12 cells to be instrumented per modem (without increasing data length).

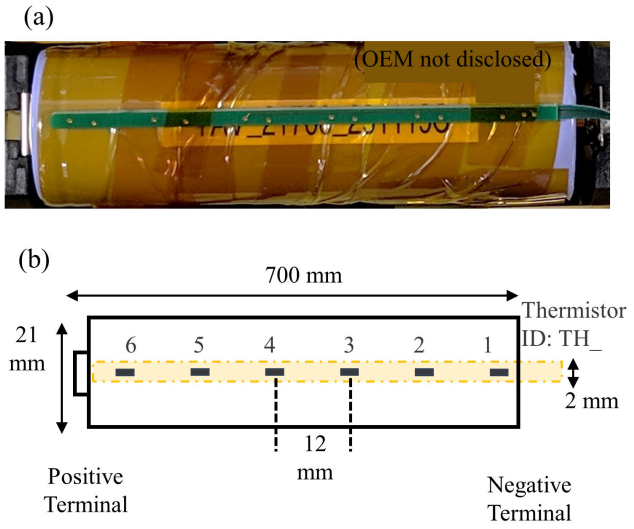

FIGURE 5. Sensors Instrumented 21700 cell, (a) photograph of semi-flex PCB fitted to cell in holder with thermistor sensors, (b) diagram showing distribution of sensors along cell can.

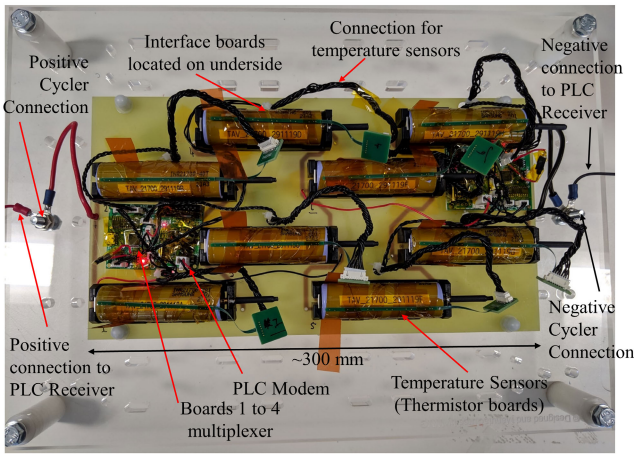

FIGURE 6. Photograph of assembled instrumented module (thermistor PCBs visible) with PLC setup. Interface boards are hidden from view (on underside of mounting board).

A complete data string, transmitted sent from one cell, consists of the board serial number, current sensor reading, 6 temperature sensor readings, voltage sensor reading, timestamp and debug data, as shown in Table 1.

D. EXPERIMENT SCENARIOS

Two test procedures were defined to enable the measurement system and PLC network to be trialed: (Configuration 1) a ∼200 min charge and discharge cycle (repeated 10× per run), with constant current rates, enabling the measurement sensor setup to be assessed; (Configuration 2) a ∼50 min experiment of transient current variation (drive cycle, based on measurements of speed-time data of a real vehicle in Coventry, UK [35]) to allow the response time and data acquisition configuration to be verified.

TABLE 1. Elements of data string transmitted from each multiplexer board (collecting data from four interface boards) over the power line.

Field Name	Data Size	Resolution
Cell IDs	19 bytes	N/A
Current Data	125 bytes	12 bit
Temperature Data	19 bytes	12 bit
Auxiliary (spare) fields	19 bytes	12 bit
Voltage Data	19 bytes	12 bit
Timestamp	8 bytes	ms runtime
Debug Data	11 bytes	N/A

Each experiment routine was performed for three repetitions, one data set from each, containing representative data, will be presented below. Figure 7 shows the current supplied and drawn from the module for each scenario (as only 4S2P layout, maximum current load set as 1 C).

IV. RESULTS AND DISUSSION

A total of 48 thermistor temperature sensors were installed (6 per cell), additionally voltage and current data was recorded for each individual cell. A reference sensor was placed for temperature (thermocouple placed on center of external can surface) on each cell. Voltage and current data recorded from the cycler is presented, alongside the data logged via the PLC network. Prior to each experiment, the module was charged to ∼95% SoC (16.5 V, considering each cell 95% SoC is ∼4.125 V). These results will verify the five hypotheses discussed previously. In this work, charging current is indicated as positive direction.

A. STEPPED CURRENT CYCLE (Configuration 1)

In this set of experiments, the cells are cycled through a periodic stepped program. The functionality of the sensors can be verified, evaluating hypotheses (i) and (ii). A set of data, shown in Figure 8 for cell 5, is recorded for each cell. Plots (a) and (c) show data logged via PLC, collected from the miniature sensors proposed for instrumenting cells. (c) shows 6 data strings, one for each of the sensors fixed to the can surface. (b) shows reference data logged from a thermocouple, placed at the centre of the cell. It is noted, the climate chamber (environment) was set to 25 °C, with no humidity control. Due to the large volume of the chamber, temperature variance within the chamber is to be expected. Baseline temperature measurements (based on the reference thermocouple data) were recorded: 25.6, 26.1, 26.0, 25.3, 24.9, 25.7, 25.2, and 25.8 °C, for cells 1 to 8 respectively.

The current data shown in Figure 8 (a) and temperature data in (b) demonstrate the surface temperature of the cell increases, as energy is charged and discharged. The peak temperature is observed at the highest charge rate (8A between 2P cells). The maximum temperature recorded by the thermistors is ∼28.4 °C (S4 and S5), while the thermocouple records a maximum of 27.8 °C. The thermocouple data closely

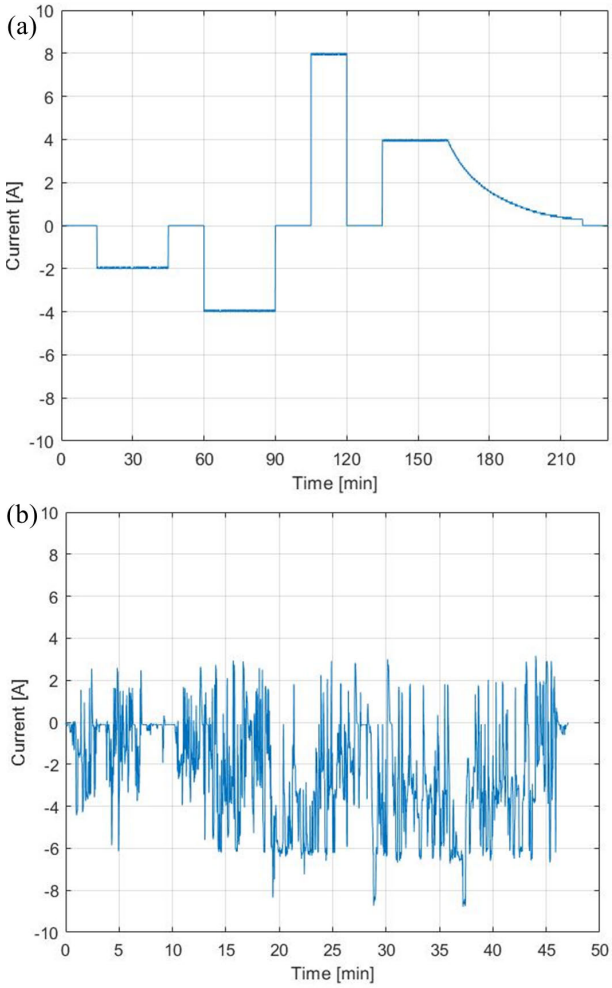

FIGURE 7. Plots of current charged (indicated as positive current) and discharged (negative) into the module (8 cells, 4S2P) during each experimental scenario, (a) Stepped cycle (1 cycle of the program), data taken from cycler log, (b) transient drive cycle experiment, data from drive cycle, 1 sample/s.

corresponds to the nearest thermistor (S3), in terms of trajectory and minimum temperature (both ∼25.0 °C baseline); the peak S3 temperature is higher (average 27.5 ° across the 10 cycles).

An enlarged view of the temperature variation across one cycle (third repetition selected) is shown in Figure 9. For each cell, three plots were extracted from the data matrix: the hottest thermistor sensor, the sensor reading of either S3 or S4 (physically closest to the reference sensor), and the reference thermocouple. The hottest sensor values generally are recorded by Sensors 5 or 6, closest to the positive tab of the cell. The data recorded by sensors 3 and 4 correspond closest to the reference sensor (located physically in the same location on the cell).

The variation of either S5 or S6 as the hottest point on the cell indicates the need to characterize individual cell configurations to identify hot spots for a particular cell. Greater variation is observed from the thermocouple, perhaps

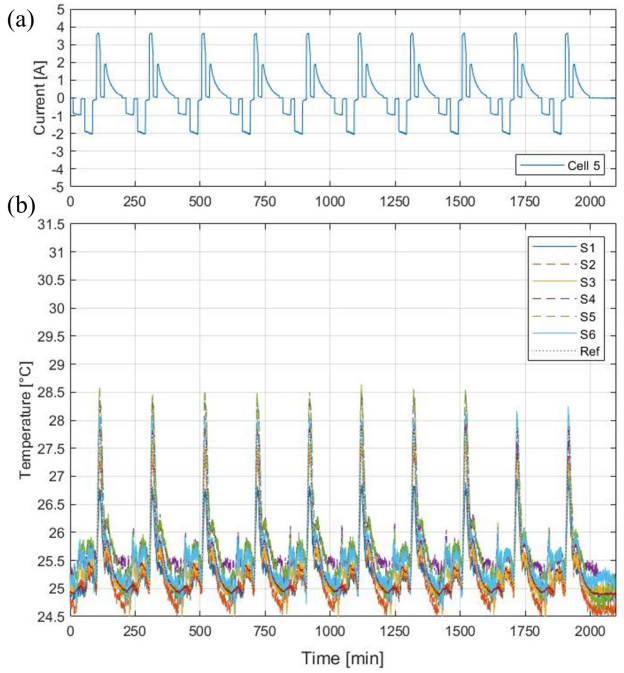

FIGURE 8. Cell 5 current and temperature data during stepped current experiment, (a) Current measured and recorded via PLC for individual cell, (b) thermistor data, recorded via PLC (6 sensors along length of cell) and reference thermocouple data (sensor located centre of cell).

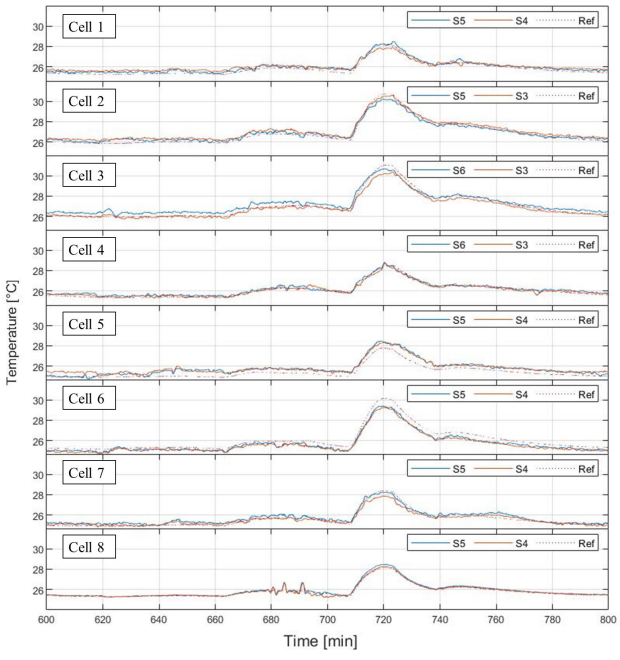

FIGURE 9. Cell temperature observed during third cycle, for each cell the sensor recording hottest values (generally S5 or S6), value closest to reference sensor (S3 or S4) and the reference thermocouple.

showing fluctuations in temperature within the climate chamber (as it operates to maintain a constant 25 °C). The thermocouple has a greater exposure to external temperature variation, while the thermistors are covered by being mounted on a PCB.

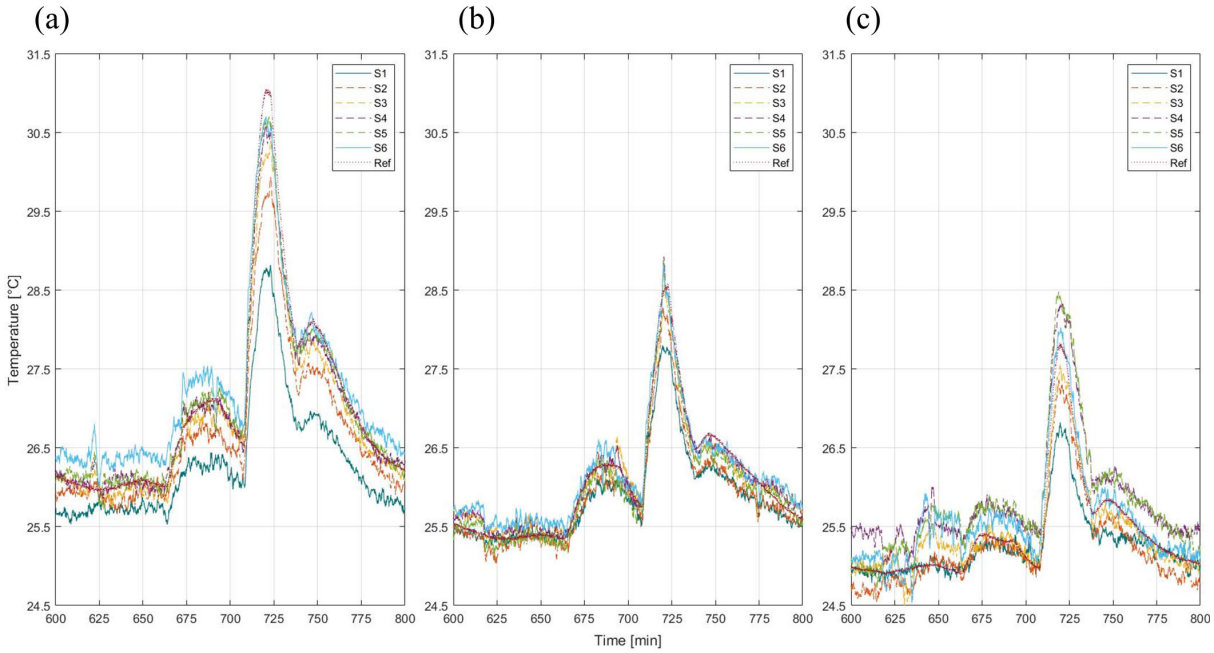

FIGURE 10. Variation of temperature recorded via thermistor PLC and reference thermocouple shown in (a), (b) and (c) for cells 3, 4 and 5, respectively.

Figure 10 shows a further enlarged view of the same cycle for cells 3, 4 and 5, in plots (a), (b) and (c), respectively. For cells 4 and 5, the thermocouple temperature corresponds to S3 throughout the cycle. Cell 3 shows larger variation, exceeding S3 temperature by ∼0.55 °C. Cell 3 reaches the highest temperatures (4.6 °C above baseline, compared to 3.6 and 3.5 °C, cells 4 and 5, respectively), confirmed by the highest thermocouple reading (31.0 °C). The thermistors along the length of cells 4 and 5 exhibit a general trend of a cooler negative terminal on the cell (S1), although S4 to S6 tend to group together (variance of ∼0.15 °C at peak temperature readings).

The thermistor PCB on cell 3 demonstrates an upward trend in temperature between S1 to S6, with the negative terminal coolest (28.8 °C), gradually increasing to S6 (30.7 °C). Regarding hypothesis (iv), this experiment demonstrates useful information can be gained about the temperature gradients along a cell surface during its operation, the majority of information can be obtained by considering the hottest point in the cell.

It is suggested a strategically placed temperature sensor, near the positive end of the cell, may provide sufficient data, although ideally internal core measurement would be preferred [19]. This reduces the bandwidth required for a communication system, and optimises the data processed by the receiver (BMS). In the case of a laboratory setup, a smart cell could identify the hottest point in the cell, and report only this data point during real-time reporting to the BMS (while logging the remaining temperature sensors in memory within the cell, for later retrieval if requested).

To reduce component cost, and intrusion into the cell, to internally instrument a cell, a reduced array of sensors may be adequate. Alternatively, for larger format cells (or pouch cells), bespoke arrangements of sensors are possible.

The hottest area of a cylindrical cell has previously been identified near the positive terminal [36], [37], although this may neglect detection of aging hot spots. The first peak in temperature (∼680 min) could be investigated further, following reports a sharp rise in temperature is observed near the end of the discharge to low state of charge, due to the increased internal resistance of the cells [38].

To verify the operation of the current sensor on each cell, the data can be summed across each pair (2P) of cells and validated against the current supplied and drawn from the module. Figure 11 (a) shows the summed data across the 10 cycles. Each pair sums to a peak charging current of 8 A (1C) and the peak discharging current (4A, 0.5 C). Figure 11 (b) shows the individual current transferred through each cell.

The charging and discharging rates of each cell in a pair are not equal, visible in the curves during peak discharge and charge, Figure 11 (b). A view of one cycle is enlarged in Figure 12, showing all 8 cells. The step changes in supplied charging current causes the currents through the cells to converge (∼700 min) and diverge (∼710 min). By monitoring the individual cell currents this effect can be quantified, and provides an understanding of the individual cell's condition [39], [40]. At the time points 685, 700 and 720 min, the SoC of the cells are approximately 52%, 63% and 86%, respectively. A smaller applied current causes an

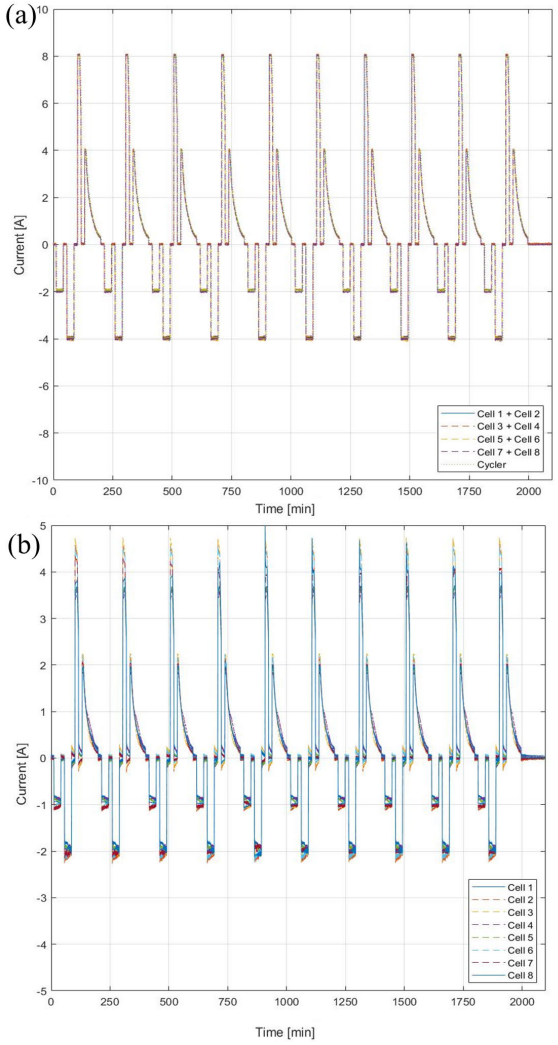

FIGURE 11. Current measured through module, (a) comparing sum of current cell pairs to cycler, (b) current observed at each individual cell.

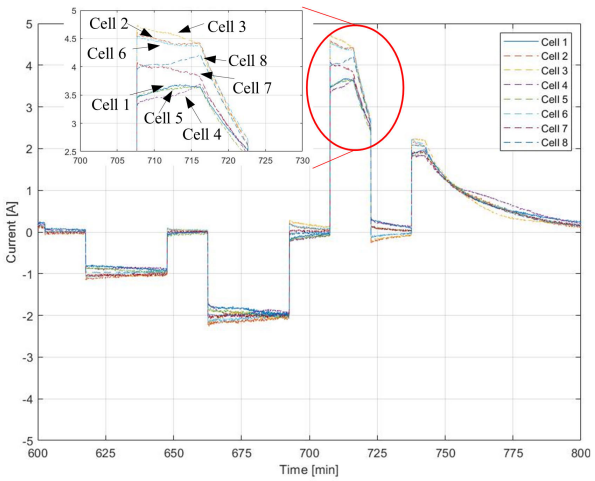

FIGURE 12. Enlarged view of one cycle (third) through individual cells, inset graph enlarges view showing varying charging rates.

inter-cell self-balancing effect to dominate the applied current to the system. However, a larger applied current demonstrates the counter effect, with a greater magnitude in current

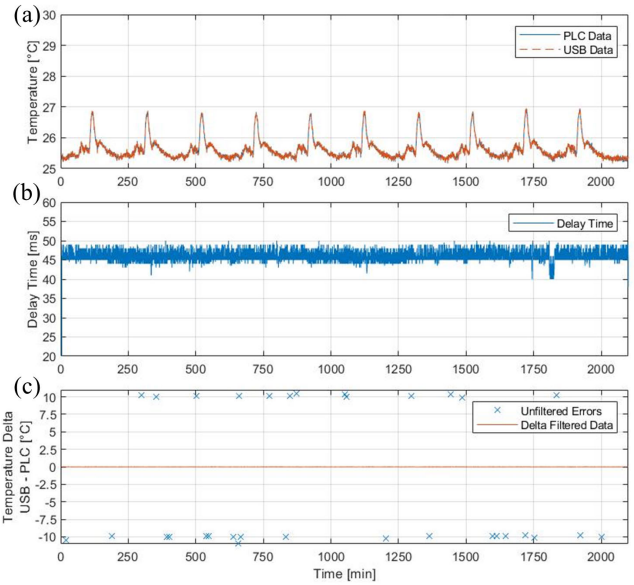

FIGURE 13. Comparison of temperature sensor data received by Cell 7 Sensor 1 recorded via dedicated wired connection and PLC link, (a) temperature sensor data, (b) delay time (dedicated-PLC) and (c) errors noted prior to filtering and after smoothing filter.

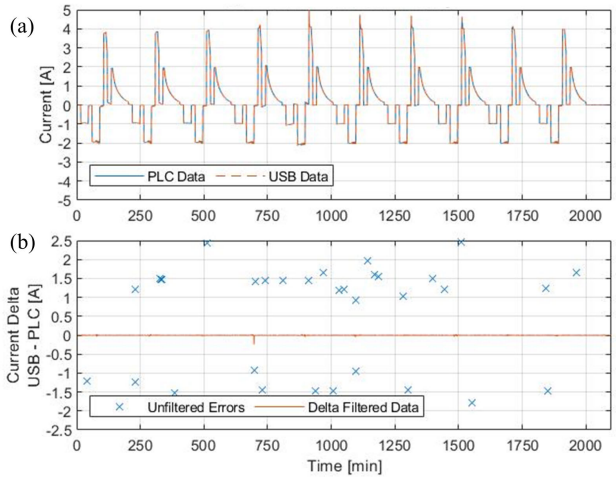

FIGURE 14. Comparing current data recorded via PLC and dedicated wired connection, (a) shows data logged by each method, (b) delta current recorded.

offsets, decreasing as the individual cell state of charges converge.

To assess hypotheses (i) and (v), the quality of the PLC link was studied. Comparative data was logged directly from the smart cell interface board (on-board microcontroller connected via dedicated USB link to data logging computer). Performance criteria were defined as BER and time delay to receive message.

Figure 13 (a) shows the logged temperature data for one thermistor (cell 7, sensor location 1), recorded via dedicated link and PLC. There is no determinable variation between the temperature logged and time recorded. The measured

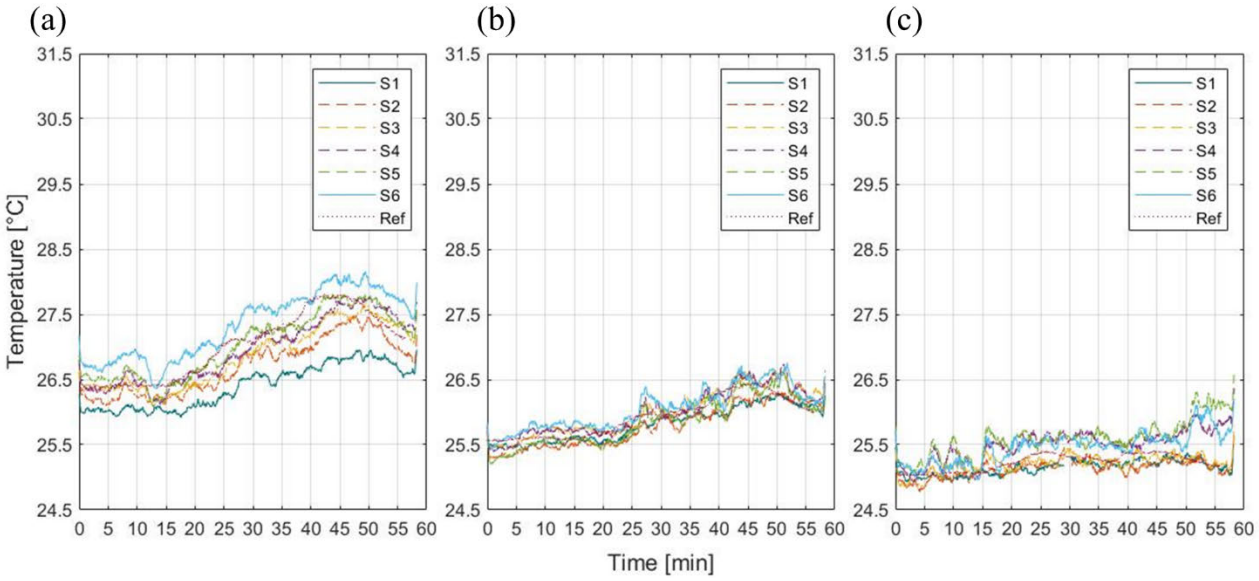

FIGURE 15. Temperature recorded (6 thermistors and 1 reference thermocouple) during transient drive cycle, (a), (b) and (c) show cells 3, 4 and 5, respectively.

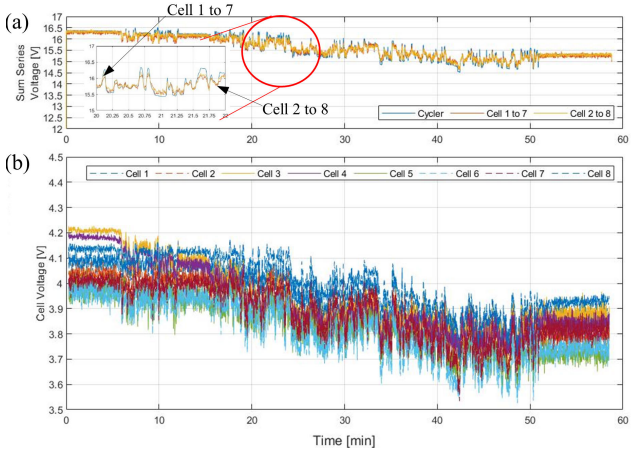

FIGURE 16. Transient voltages recorded during drive cycle, (a) sum of voltages of series four cells compared to cycler data, (b) individual cell voltages logged via PLC.

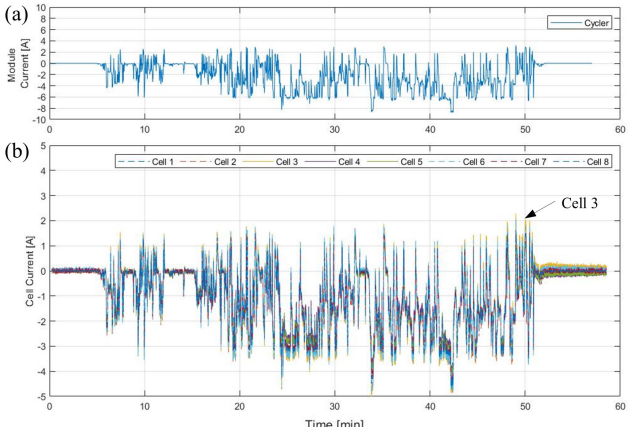

FIGURE 17. Transient currents recorded, (a) cycler data, (b) data from individual cells.

time delay, Figure 13 (b), is calculated via comparison of the timestamps when a given data (from all the cells sensors together) received by the data logging computer. The average delay time was calculated as 45.6 ms, considering data from all sensors (cell 7).

The temperature delta between the dedicated wired vs PLC links is shown in Figure 13 (c). During the experiment, 32 bit errors occurred (0.002%), leading to temperature variations of >10 °C for the erroneous measurement point. These can be filtered out (median filter) to exclude abrupt variation in temperature. These bit errors include errors introduced during every part of the transmission process, i.e. interface board to multiplexer board (Universal Asynchronous Receiver/Transmitter, UART), multiplexer to modem (UART), the power line transmission and finally receiving PLC modem to microcontroller (UART). Opposed to the dedicated wired link (interface board directly to computer via USB). In future work, the integrity of the data could be checked when at the multiplexer or modem boards, to allow bit errors introduced via the UART transfers to be detached from those introduced with the PLC stage.

A similar comparison is shown in Figure 14 for the current sensor installed on cell 7. (a) demonstrates data is intact transmitted via PLC compared to the reference wired link. (b) shows the bit errors introduced due to the communication process. The majority of the errors are filtered out, and do not impact the current readings.

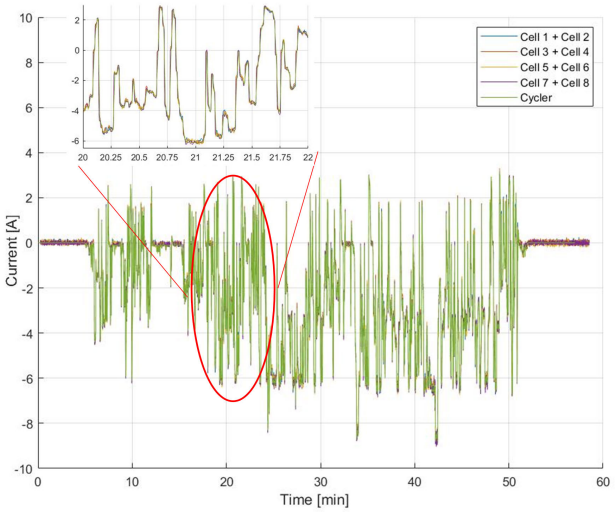

FIGURE 18. Transient current data summed across cell pairs relative to supplied module data, inset plot shows enlarged 2 minute period.

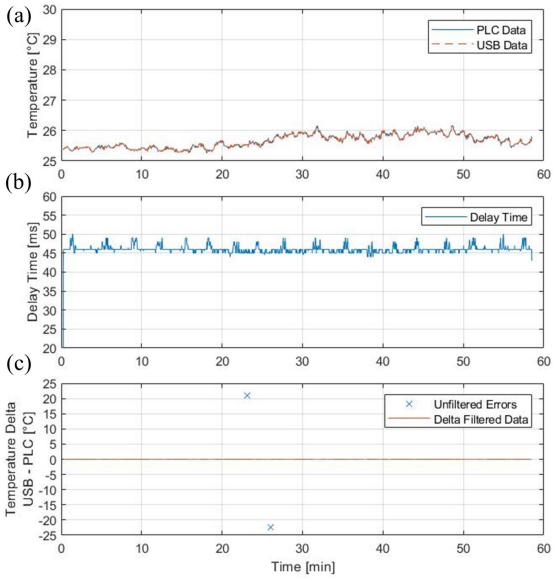

FIGURE 19. Comparison of data recorded via PLC and dedicated wired (USB) link; (a) temperature data (Cell 7 sensor 1) comparison, (b) delay time between messages being received, (c) Errors noted prior to filtering (temperature delta also shown after filtering).

B. TRANSIENT DRIVE CYCLE (CONFIGURATION 2)

To verify hypotheses (ii) and (iii), experimental configuration 2 subjects the module to a transient 'drive cycle' profile, with rapid (1 s) variation in current drawn and charged. The cell surface temperature variation is minimal throughout the experiment (most cells < 2 °C variation). Figure 15 shows temperature variation (data logged with thermistors and reference thermocouple) for cells 3, 4 and 5 in (a), (b) and (c), respectively.

Transient voltage data is shown in Figure 16. (a) compares the sum of the two series strings of cells against the module reading. The PLC board data, available at higher sampling rate, corresponds to the reference data. Individual cell voltages are shown to provide greater insight into module health, as demonstrated in (b). Cell 3 and 4 (parallel cells) have notably higher potentials (e.g. ∼4.2 V when expected 95% SoC). This indicates the cells could have a greater aging effect compared to counterpart cells (e.g. cell 5), or have reduced capacity (reduced retained capacity). These increased cell voltages correspond to the higher temperatures during cycling observed in Figure 15 (a) and (b), i.e. peak readings ∼27.8, 26.7 and 25.8 °C, respectively for cells 3, 4 and 5.

The transient current data was recorded using the cycler output and individual cell sensors. Figure 17 compares cycler data (a) with cell data (b).

Cell 3 is again noted as receiving a higher current (as well as being hottest, and noted as lowest SoH) while charging (e.g. peak 2.0 versus 1.8 A to neighbouring cells), justifying the need to implement improved parameter sensing in a module.

To verify the currents through each pair of cells summed to the recorded input data, Figure 18 compare pair summed values to the cycler log. Greater sampling resolution is available from the PLC data (inset plot). All current voltages sum correctly, with negligible variation.

A comparison of data recorded via a dedicated wired USB link and via PLC was performed; Figure 19 (a) shows the data recorded for cell 7 sensor 1 (thermistor). The transmission delay between the dedicated wired link and PLC connection was calculated as 49 ms, shown in (b). Inspecting the raw data prior to filtering, 2 errors are located for this stream (c). A total BER of 0.003% was noted, a fraction of the minimum accepted 10^{-4} rate defined by the G3 Alliance [41].

This rate is similar to configuration 1, although more significant bits were corrupted, leading to larger variations in apparent temperature reading. A BER of 3.1×10^{-9} has been reported for CAN bus communications in normal conditions [42]. Further work will involve improving verification of received data on the microcontrollers, to minimise bit losses during data handling. Figure 20 demonstrates the successful transfer of the data via PLC, relative to USB dedicated link. The data are intact, shown in (a), while a handful of errors are introduced (b).

These experiments have investigated the use of PLC within a small module and resolved our hypotheses. We propose such a system would benefit pack and cell design, where key sensor locations can be identified (e.g. temperature sensors). The data collected over the powerline was not corrupted (i), and did not notably determent the performance of the module. The selected miniature sensors offered comparable data to reference instrumentation (ii), demonstrating the viability of installing sensors in a module for laboratory testing.

The bandwidth of the PLC (iii) system limited the sampling rate (4 or 6 Hz). Faster sampling rates could be achieved the prioritising data (e.g. when abnormal temperatures detected) to enable further data to be gathered from an individual cell. The bi-directional communication enabled these parameters to be controlled, although not autonomously.

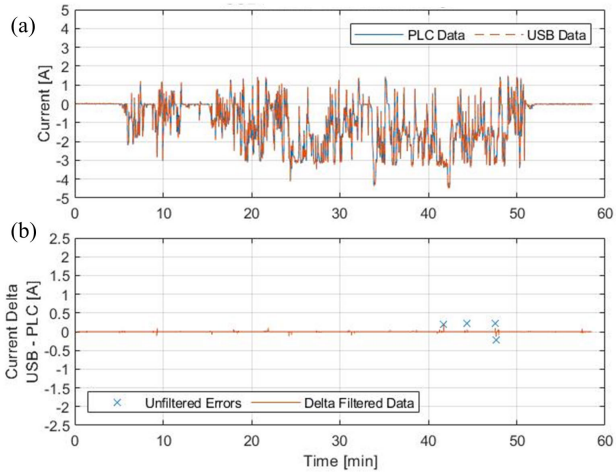

FIGURE 20. Comparison of data recorded via PLC and wired link; (a) current data (Cell 7), (b) errors recorded pre/post filtering.

Hotter locations (i.e. towards the positive terminal) along the surface of a cell were identified (iv), particularly the cells experiencing greater current demand and higher voltages. The data collected over PLC was delayed (never exceeding < 50 ms) compared to a dedicated wired connection (v). This is considered comparable to a CAN system, with a common message rate of between 10 and 50 ms, for key battery parameters. This delay could be minimised by fitting a PLC modem to each individual cell, avoiding the delay entailed with collecting data from 4 separate boards and multiplexing the output to a single PLC modem.

V. CONCLUSION

This work has demonstrated PLC is a viable communication method (in terms of transmission speed, reliability, bandwidth) to instrument cells in a small module. Current generation cells do not contain circuitry nor sensors to record parameters nor understand their performance (e.g. age, lifetime). This work demonstrated future generation EVs could benefit from smart cells, where owners would benefit from obtaining the full potential (charging/discharging rates, lifetime) possible from their vehicles. Manufacturers would benefit from being able to develop packs containing sufficient sensors in key locations to safely maximise pack performance and lifetime. The current sensor configuration (with temperature sensors 0.3×0.6 mm size) demonstrates the reduced size sensor networks possible, compared to using traditional thermocouple sensors.

A PLC system was constructed, consisting of 2 low bandwidth (56 kbps) powerline modems (SIG60, 150 mW required per board) and 8 sensor interface boards (100 mW per board). Two multiplexer boards acquired data from 4 sensor interface boards, which were then transmitted via the PLC modem. 8 cells were instrumented in a 4S2P configuration, enabling temperature (6 thermistors installed along length of cell), current and voltage data to be logged. A total of 9 data records were transmitted from each interface board, making a total of 36 per multiplexer. In the 4S2P configuration here, all the comprehensive sensor layout demonstrated in a laboratory setting, reasonable detail (10 mm resolution) cell surface temperature is possible. However, to increase the number of cells instrumented without increasing data load, the system could be distributed with 3 channels per board (temperature, voltage, current), enabling 12 cells to be instrumented per modem, without changing the PLC configuration. The low bandwidth modems provided sufficient bandwidth to obtain data from all these sensors at 4 Hz and 6 Hz sampling rates (standard or transient settings).

Reliable data sampling was observed through testing a stepped charge/discharge cycle (200 mins, 5m samples, BER $\sim$0%). A time delay compared to a dedicated wire connection of $\sim$45 ms was observed, sufficient to enable rapid notification of a temperature increase (sampling time could be improved in further work through prioritisation).

Transient drive cycle experiments verified the functionality of the miniature sensors for real-time measurements (current sensor tracked cycle, logging at 6 Hz, typical cycle stepped at 1 Hz). Variations were observed between cell SoC (e.g. 95% SoC 4.2 V compared to 4.125 V) demonstrating the need to understand individual cell aging and capacities.

VI. FURTHER WORK

It is proposed the system is further miniaturised (combining the sensor interface boards with a PLC modem per cell), enabling the wire-free concept of a smart cell monitoring system to be realised. This work has formed proof-of-concept a PLC system is resilient to general cycling with real cells subjected to a real-world drive cycle.

A. INTEGRATION WITH SMART CELLS

Data were collected from the miniature sensors using a low-cost microcontroller, utilising a 12-bit ADC. To maintain a cost-effective smart cell, minimising component costs is important, although it is proposed a dedicated ADC could improve sensor resolution (and reduce spurious noise spikes). This may be useful for prototype smart cells to be used in pack development and laboratory studies.

In the current setup, a limitation was noted; the SoC of each cell was not reduced below 50% ($\sim$3.75 V), to ensure correct operation of the interface circuitry (using a low-dropout 3.3 V regulator, total power consumption $\sim$100 mW per board). Correct functionality was observed until the drop out voltage (3.34 V); below this threshold false ADC readings were obtained, i.e. erroneous sensor measurements. The operating voltage range of each sensor interface board must be extended to encompass the cells SoC from 0 to 100%. This was trialled using a buck-boost regulator, although this component reduced system power efficiency (power consumption reaching 165 mW observed), and was excluded from this current work.

Externally instrumented cells were utilised to provide proof-of-concept smart cells. To demonstrate the reduced complexity and reduction in wiring loom possible with PLC,

our next research topics include embedding the sensors in-situ inside the core of the cells. Core temperature is desirable for modelling studies, providing a reflection of the cells operation at a faster rate, compared to surface measurements. Working with flexible PCBs could enable placement of sensors at different locations within the cell and different planes, to help identify the key areas to detect the formation of hot spots.

B. PLC DEVELOPMENT

The PLC network in this study was subjected to transient current profiles and varying cell SoC. Further work includes further reliability testing, involving perhaps white noise testing and interference noise sources.

The low-bandwidth configuration was sufficient to enable 8 cells to be comprehensively instrumented and report to a central data logger at 6 Hz. This is sufficient for monitoring transient behaviour, although greater sampling rates (order of 1 kHz) may be desired. Higher bandwidth PLC systems are available, although demand greater power consumption (initial testing suggests 1 W per modem). This entails clusters of cells should be instrumented and linked to one modem.

We propose developing a miniature low-bandwidth PLC modem combined with sensor interface hardware to enable a cell to be instrumented and communicate with a data logger without external wiring. This will allow the bit error rate of the PLC network to be assessed per cell, opposed to current work (which requires several UART inter-board networks). Fixed sampling rates were used in this work; it is proposed adaptive smart sampling is used, thus enabling an event (i.e. temperature increase) to automatically trigger faster sampling, so the event can be monitored.

A dedicated USB link was used to assess the errors introduced with the PLC network. This was selected to reduce the possible errors occurring linking the sensor interface board to a secondary communication protocol (microcontroller has integrated USB communication). To verify reliability against accepted standards, a comparison against CAN, SPI or wireless technologies is proposed.

C. INTEGRATION WITH LARGER SCALE MODULES AND BMS

This work demonstrated functionality at a small module level with every cell instrumented. The PLC network structure is adaptable, thus a pattern of cells could be instrumented in a module, thereby reducing the component cost associated with smart cells.

To demonstrate the resilience of the network to node failure abuse testing is required. A failure of a cell (i.e. due to damage or thermal runaway) should not affect the ability of other cells to communicate.

This work forms a proof-of-concept study that instrumented cells via PLC are suitable for laboratory testing and data acquisition. Our future work, demonstrating lower-cost, physically smaller and higher resolution sensing will help showcase the path towards future smart cells.

REFERENCES

[1] S. Küfeoğlu and D. Khah Kok Hong, "Emissions performance of electric vehicles: A case study from the United Kingdom," *Appl. Energy*, vol. 260, Feb. 2020, Art. no. 114241, doi: 10.1016/j.apenergy.2019.114241.
[2] J. Ahuja, L. Dawson, and R. Lee, "A circular economy for electric vehicle batteries: Driving the change," *J. Property, Planning Environ. Law*, vol. 12, no. 3, pp. 235–250, Aug. 2020, doi: 10.1108/JPPEL-02-2020-0011.
[3] C. Brand, J. Anable, I. Ketsopoulou, and J. Watson, "Road to zero or road to nowhere? Disrupting transport and energy in a zero carbon world," *Energy Policy*, vol. 139, Apr. 2020, Art. no. 111334, doi: 10.1016/j.enpol.2020.111334.
[4] M. Giansoldati, L. Rotaris, M. Scorrano, and R. Danielis, "Does electric car knowledge influence car choice? Evidence from a hybrid choice model," *Res. Transp. Econ.*, vol. 80, May 2020, Art. no. 100826, doi: 10.1016/j.retrec.2020.100826.
[5] S. Fluchs, "The diffusion of electric mobility in the European union and beyond," *Transp. Res. D, Transp. Environ.*, vol. 86, Sep. 2020, Art. no. 102462, doi: 10.1016/j.trd.2020.102462.
[6] Department of Transport. (2020). *Cars VEH02 Statistical Data Set*. UK Government. Accessed: Oct. 2020. [Online]. Available: https://www.gov.uk/government/statistical-data-sets/veh02-licensed-cars
[7] H. Greim, "Diesel engine emissions: Are they no longer tolerable?" *Arch. Toxicol.*, vol. 93, no. 9, pp. 2483–2490, Sep. 2019, doi: 10.1007/s00204-019-02531-5.
[8] A. Alberini, V. Di Cosmo, and A. Bigano, "How are fuel efficient cars priced? Evidence from eight EU countries," *Energy Policy*, vol. 134, Nov. 2019, Art. no. 110978, doi: 10.1016/j.enpol.2019.110978.
[9] M. Hussaini and M. Scholz, "Exploring low carbon transition pathways for the UK road transport sector," *Transp. Planning Technol.*, vol. 40, no. 7, pp. 796–811, Oct. 2017, doi: 10.1080/03081060.2017.1340024.
[10] T. Muneer, R. Milligan, I. Smith, A. Doyle, M. Pozuelo, and M. Knez, "Energetic, environmental and economic performance of electric vehicles: Experimental evaluation," *Transp. Res. D, Transp. Environ.*, vol. 35, pp. 40–61, Mar. 2015, doi: 10.1016/j.trd.2014.11.015.
[11] X. Lin, H. E. Perez, J. B. Siegel, and A. G. Stefanopoulou, "Robust estimation of battery system temperature distribution under sparse sensing and uncertainty," *IEEE Trans. Control Syst. Technol.*, vol. 28, no. 3, pp. 753–765, May 2020, doi: 10.1109/tcst.2019.2892019.
[12] J. B. Quinn, T. Waldmann, K. Richter, M. Kasper, and M. Wohlfahrt-Mehrens, "Energy density of cylindrical li-ion cells: A comparison of commercial 18650 to the 21700 cells," *J. Electrochem. Soc.*, vol. 165, no. 14, pp. A3284–A3291, 2018, doi: 10.1149/2.0281814jes.
[13] A. Misra, "Energy storage for electrified aircraft: The need for better batteries, fuel cells, and supercapacitors," *IEEE Electrific. Mag.*, vol. 6, no. 3, pp. 54–61, Sep. 2018, doi: 10.1109/MELE.2018.2849922.
[14] M. Weiss, K. C. Cloos, and E. Helmers, "Energy efficiency trade-offs in small to large electric vehicles," *Environ. Sci. Eur.*, vol. 32, no. 1, p. 46, Dec. 2020, doi: 10.1186/s12302-020-00307-8.
[15] Y. Barsukov and J. Qian, *Battery Power Management for Portable Devices*. Boston, MA, USA: Artech House, 2013.
[16] J. G. Zhu, Z. C. Sun, X. Z. Wei, and H. F. Dai, "A new lithium-ion battery internal temperature on-line estimate method based on electrochemical impedance spectroscopy measurement," *J. Power Sources*, vol. 274, pp. 990–1004, Jan. 2015, doi: 10.1016/j.jpowsour.2014.10.182.
[17] W. Waag, S. Käbitz, and D. U. Sauer, "Experimental investigation of the lithium-ion battery impedance characteristic at various conditions and aging states and its influence on the application," *Appl. Energy*, vol. 102, pp. 885–897, Feb. 2013, doi: 10.1016/j.apenergy.2012.09.030.
[18] T. Amietszajew, "Hybrid thermo-electrochemical *In Situ* instrumentation for lithium-ion energy storage," *Batteries Supercaps*, vol. 2, no. 11, pp. 934–940, Nov. 2019, doi: 10.1002/batt.201900109.
[19] G. Zhang, L. Cao, S. Ge, C.-Y. Wang, C. E. Shaffer, and C. D. Rahn, "*in situ* measurement of radial temperature distributions in cylindrical li-ion cells," *J. Electrochem. Soc.*, vol. 161, no. 10, pp. A1499–A1507, Jul. 2014, doi: 10.1149/2.0051410jes.
[20] A. Fortier, M. Tsao, N. Williard, Y. Xing, and M. Pecht, "Preliminary study on integration of fiber optic Bragg grating sensors in li-ion batteries and *in situ* strain and temperature monitoring of battery cells," *Energies*, vol. 10, no. 7, p. 838, Jun. 2017, doi: 10.3390/en10070838.
[21] J. Li, J. Klee Barillas, C. Guenther, and M. A. Danzer, "A comparative study of state of charge estimation algorithms for LiFePO4 batteries used in electric vehicles," *J. Power Sources*, vol. 230, pp. 244–250, May 2013, doi: 10.1016/j.jpowsour.2012.12.057.

[22] *Global Technical Regulation on the Electric Vehicle Safety (EVS)*, United Nations Economic Commission for Europe, Geneva, Switzerland, 2018.
[23] D. P. Finegan, J. Darst, W. Walker, Q. Li, C. Yang, R. Jervis, T. M. M. Heenan, J. Hack, J. C. Thomas, A. Rack, D. J. L. Brett, P. R. Shearing, M. Keyser, and E. Darcy, "Modelling and experiments to identify high-risk failure scenarios for testing the safety of lithium-ion cells," *J. Power Sources*, vol. 417, pp. 29–41, Mar. 2019, doi: 10.1016/j.jpowsour.2019.01.077.
[24] H. Maleki, H. Wang, W. Porter, and J. Hallmark, "Li-ion polymer cells thermal property changes as a function of cycle-life," *J. Power Sources*, vol. 263, pp. 223–230, Oct. 2014, doi: 10.1016/j.jpowsour.2014.04.033.
[25] R. R. Richardson, P. T. Ireland, and D. A. Howey, "Battery internal temperature estimation by combined impedance and surface temperature measurement," *J. Power Sources*, vol. 265, pp. 254–261, Nov. 2014, doi: 10.1016/j.jpowsour.2014.04.129.
[26] A. P. Talie, W. A. Pribyl, and G. Hofer, "Electric vehicle battery management system using power line communication technique," in *Proc. 14th Conf. Ph.D. Res. Microelectron. Electron. (PRIME)*, Jul. 2018, pp. 225–228, doi: 10.1109/PRIME.2018.8430304.
[27] I. Ouannes, P. Nickel, J. Bernius, and K. Dostert, "Physical layer performance analysis of power line communication (PLC) applied for cell-wise monitoring of automotive lithium-ion batteries," in *Proc. 18th Int. OFDM Workshop (InOWo)*, Aug. 2014, pp. 136–143.
[28] A. P. Talei, W. A. Pribyl, and G. Hofer, "Wide frequency range impedance measurement of a li-ion prismatic cell for power line communication technique," in *Proc. 16th Int. Conf. Synth., Modeling, Anal. Simulation Methods Appl. Circuit Design (SMACD)*, Jul. 2019, pp. 109–112, doi: 10.1109/smacd.2019.8795281.
[29] I. Ouannes, P. Nickel, and K. Dostert, "Cell-wise monitoring of Lithium-ion batteries for automotive traction applications by using power line communication: Battery modeling and channel characterization," in *Proc. 18th IEEE Int. Symp. Power Line Commun. Appl.*, Mar./Apr. 2014, pp. 24–29, doi: 10.1109/ISPLC.2014.6812322.
[30] M. Lee, J. Lee, I. Lee, J. Lee, and A. Chon, "Wireless battery management system," in *Proc. World Electr. Vehicle Symp. Exhib. (EVS)*, Nov. 2013, pp. 1–5, doi: 10.1109/EVS.2013.6914889.
[31] M. M. Wenger, R. Filimon, V. R. H. Lorentz, and M. März, "A robust contactless capacitive communication link for high power battery systems," in *Proc. IEEE 23rd Int. Symp. Ind. Electron. (ISIE)*, Jun. 2014, pp. 1766–1772, doi: 10.1109/ISIE.2014.6864882.
[32] S. A. Mathew, R. Prakash, and P. C. John, "A smart wireless battery monitoring system for electric vehicles," in *Proc. 12th Int. Conf. Intell. Syst. Design Appl. (ISDA)*, Nov. 2012, pp. 189–193, doi: 10.1109/ISDA.2012.6416535.
[33] S. Barmada, M. Raugi, M. Tucci, Y. Maryanka, and O. Amrani, "PLC systems for electric vehicles and smart grid applications," in *Proc. IEEE 17th Int. Symp. Power Line Commun. Appl.*, Mar. 2013, pp. 23–28, doi: 10.1109/ISPLC.2013.6525819.
[34] T. A. Vincent and J. Marco, "Development of smart battery cells through sensor instrumentation and in-vehicle power line communication," in *Proc. IEEE Int. Symp. Power Line Commun. Appl. (ISPLC)*, May 2020, pp. 1–5, doi: 10.1109/ISPLC48789.2020.9115411.
[35] Yamar Electronics Ltd. *SIG60 Datasheet*. Accessed: Oct. 2020. [Online]. Available: https://www.yamar.com/
[36] Z. Wang, J. Ma, and L. Zhang, "Finite element thermal model and simulation for a cylindrical li-ion battery," *IEEE Access*, vol. 5, pp. 15372–15379, Jul. 2017, doi: 10.1109/ACCESS.2017.2723436.
[37] C. Alaoui, "Thermal management for energy storage system for smart grid," *J. Energy Storage*, vol. 13, pp. 313–324, Oct. 2017, doi: 10.1016/j.est.2017.07.027.
[38] D. Worwood, R. Algoo, R. J. McGlen, J. Marco, and D. Greenwood, "A study into different cell-level cooling strategies for cylindrical lithium-ion cells in automotive applications," *Int. J. Powertrains*, vol. 7, nos. 1–3, pp. 199–226, 2018, doi: 10.1504/IJPT.2018.090381.
[39] E. Hosseinzadeh, "Quantifying cell-to-cell variations of a parallel battery module for different pack configurations," *Appl. Energy*, vol. 282, Jan. 2021, Art. no. 115859.
[40] T. Bruen and J. Marco, "Modelling and experimental evaluation of parallel connected lithium ion cells for an electric vehicle battery system," *J. Power Sources*, vol. 310, pp. 91–101, Apr. 2016, doi: 10.1016/j.jpowsour.2016.01.001.
[41] I. Elfeki, S. Jacques, I. Aouichak, T. Doligez, Y. Raingeaud, and J.-C. Le Bunetel, "Characterization of narrowband noise and channel capacity for powerline communication in france," *Energies*, vol. 11, no. 11, p. 3022, Nov. 2018, doi: 10.3390/en11113022.
[42] J. Ferreira and J. Ferreira, "An experiment to assess bit error rate in CAN," in *Proc. 3rd Int. Workshop Real-Time Netw. (RTN*, 2004, pp. 15–18, doi: 10.1.1.124.9768.

TIMOTHY A. VINCENT received the degree (Hons.) in electronic engineering from the University of Warwick, Coventry, U.K., in 2013, and the Ph.D. degree in electronic engineering from the School of Engineering, University of Warwick, in 2017.

He is currently working as a Senior Research Fellow with the WMG, University of Warwick. His research interests include miniature sensors, communication networks for vehicular applications, and instrumenting smart cells.

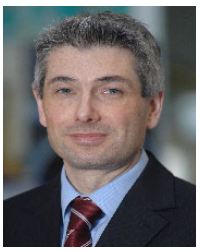

JAMES MARCO received the D.Eng. degree from the University of Warwick, in 2000. He is currently employed at the University of Warwick as a Professor of battery systems engineering, where he leads a research group focused on battery characterization, modeling, and control. His research interest includes the challenge of scaling-up individual battery cells to complete energy storage systems. Example areas include: model, control, and experimental design to quantify electro-thermal heterogeneity at cell and system level; and methods to extend battery useful life through repurposing and re-use.